Nuclear fragmentation and charge-exchange reactions induced by pions in the Δ-resonance region

Zhao-Qing Feng*
Institute of Modern Physics, Chinese Academy of Sciences, Lanzhou 730000, People's Republic of China
(Received 5 September 2016; revised manuscript received 11 October 2016; published 18 November 2016)

The dynamics of the nuclear fragmentations and the charge exchange reactions in pion-nucleus collisions near the Δ(1232) resonance energies has been investigated within the Lanzhou quantum molecular dynamics transport model. An isospin-, momentum-, and density-dependent pion-nucleon potential is implemented in the model, which influences the pion dynamics, in particular the kinetic energy spectra, but weakly impacts the fragmentation mechanism. The absorption process in pion-nucleon collisions to form the Δ(1232) resonance dominates the heating mechanism of the target nucleus. The excitation energy transferred to the target nucleus increases with the pion kinetic energy and is similar for both π^-- and π^+-induced reactions. The magnitude of fragmentation of the target nucleus weakly depends on the pion energy. The isospin ratio in the pion double-charge exchange is influenced by the isospin ingredient of target nucleus.

DOI: 10.1103/PhysRevC.94.054617

I. INTRODUCTION

The dynamics of pions is of importance in understanding the transportation process in heavy-ion collisions and in hadron-induced reactions, which also contributes other particle production as the main reaction channels, such as η, strange particles, etc. Pion production in heavy-ion collisions near threshold energies has been investigated for extracting the high-density behavior of the nuclear symmetry energy (isospin asymmetric part of an equation of state) [1–4]. The dynamics of pions produced in heavy-ion collisions is a complicated process, which is related to the pion-nucleon and Δ(1232)-nucleon interactions, the decay of resonances, etc. The in-medium properties of pions and Δ(1232) are not well understood up to now and are related to the isospin effects. The in-medium effects of pions in heavy-ion collisions have been studied in Refs. [5,6] for threshold energy corrections and in Refs. [7–10] for the pion optical potential. The baryon density of the pions produced varies with the evolution dynamics in nucleus-nucleus collisions, in which parts of pions are created above normal nuclear density. However, the pion-nucleus reactions have advantages in investigating the pion and Δ(1232) properties in nuclear medium around the saturation density. On the other hand, the energy deposition in the pion-induced reactions would be helpful in exploring the nuclear explosion of highly excited nucleus.

In the past four decades, pion-nucleus collisions at the Δ-resonance energies have been extensively investigated within the meson factories, i.e., the Los Alamos Meson Physics Facility (LAMPF) in New Mexico, USA [11–15]; the Paul Scherrer Institute (PSI) in Villigen, Switzerland [16]; the Tri-University Meson Facility (TRIUMF) in Vancouver, Canada [17]; and the superconducting kaon spectrometer (SKS) at KEK 12-GeV PS, Japan [18]. Several theoretical approaches have been developed for understanding pion-induced nuclear reactions [19–21]. The energy released by pion-nucleon collisions heats the target nucleus. Consequently, fast-nucleon emission, particle evaporation, intermediate-mass fragments, fission, etc., will proceed. A number of nuclides are produced tending to the line of β stability [11]. In this work, a microscopic transport approach is used to describe the pion-nucleus collisions in the Δ-resonance energies. The charge-exchange reactions and fragmentation mechanism of the target nucleus are particularly concentrated on.

II. BRIEF DESCRIPTION OF THE MODEL

The Lanzhou quantum molecular dynamics (LQMD) model is used to investigate the nuclear dynamics induced by pions in the Δ-resonance region for the first time. The isospin physics, particle production, in-medium properties of hadrons, (hyper-)fragment production etc., in heavy-ion collisions and antiproton-induced (proton-induced) reactions have been investigated within the model [22–24]. I implemented an isospin-, density-, and momentum-dependent mean-field potential based on the Skyrme forces for nucleons and resonances. The optical potentials for hyperons and kaons in nuclear medium are derived from the effective Lagrangian approaches. In the model, all possible reaction channels in hadron-hadron collisions are included, i.e., charge-exchange reactions, elastic and inelastic collisions by distinguishing isospin effects, annihilation reactions in collisions of antiparticles and particles, etc. The temporal evolutions of the hadrons under the self-consistently generated mean-field potentials are governed by Hamilton's equations of motion.

The pion dynamics is influenced by the mean-field potential in nuclear medium. The potential is composed of the Coulomb interaction between the charged particles and the pion-nucleon potential. The optical potential is evaluated from the in-medium energy of pions: $V_\pi^{\rm opt}(\mathbf{p}_i,\rho_i) = \omega_\pi(\mathbf{p}_i,\rho_i) - \sqrt{m_\pi^2 + \mathbf{p}_i^2}$. The isoscalar and isovector contributions to the pion energy are included as follows [25]:

$$\omega_\pi(\mathbf{p}_i,\rho_i) = \omega_{\rm isoscalar}(\mathbf{p}_i,\rho_i) + C_\pi \tau_z \delta(\rho/\rho_0)^{\gamma_\pi}. \quad (1)$$

The coefficient $C_\pi = \rho_0\hbar^3/(4f_\pi^2) = 36$ MeV is taken from fitting the experimental data of pion-nucleus scattering. The isospin quantities are taken to be $\tau_z = 1$, 0, and -1 for

*fengzhq@impcas.ac.cn

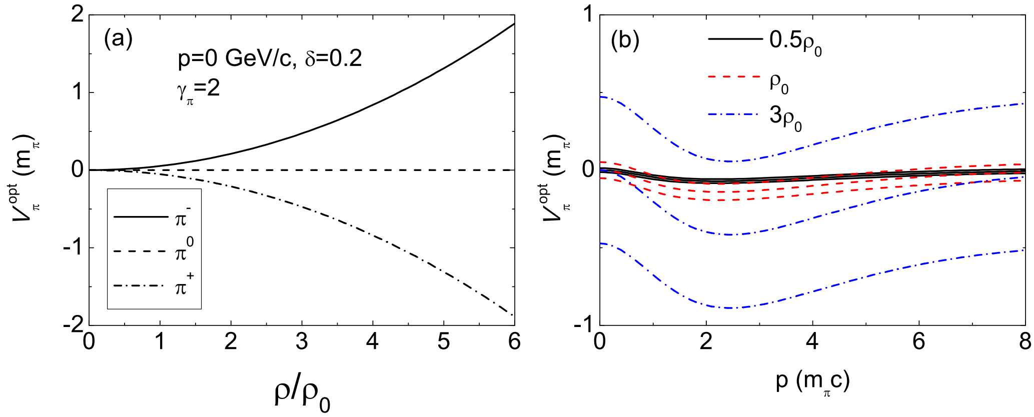

FIG. 1. Momentum and density dependence of the pion optical potential in dense nuclear matter with the isospin asymmetry of $\delta = 0.2$.

π^-, π^0, and π^+, respectively. The isospin asymmetry $\delta = (\rho_n - \rho_p)/(\rho_n + \rho_p)$ and the quantity γ_π adjusts the stiffness of isospin splitting of the pion-nucleon potential. We take $\gamma_p = 2$ in the work. The isoscalar part of the pion self-energy in the nuclear medium is evaluated via the Δ-hole model. Shown in Fig. 1 is the optical potential as a function of the baryon density and a function of the pion momentum, respectively. It should be noticed that the potential reaches the minimum at the Δ-resonance energy, i.e., $E_{\mathrm{lab}} = 0.19$ GeV or $p = 0.298$ GeV/c, which dominates the pion dynamics and enhances the pion absorption in nuclear medium.

The probability in two-particle collisions to a channel is performed by using a Monte Carlo procedure via the relative distance smaller than the scattering radius. The channels associated with the pion-induced reactions are as follows:

$$N\pi \leftrightarrow \Delta, \quad N\pi \leftrightarrow N^*, \quad NN\pi(s-\mathrm{state}) \leftrightarrow NN,$$
$$N\Delta \leftrightarrow NN, \quad NN^* \leftrightarrow NN, \quad \Delta\Delta \leftrightarrow NN. \tag{2}$$

The momentum-dependent decay widths are used for the resonances of $\Delta(1232)$ and $N^*(1440)$ [26]. We have taken a constant width of $\Gamma = 150$ MeV for the $N^*(1535)$ decay. The cross section of pion-nucleon scattering is evaluated with the Breit-Wigner formula in the following form:

$$\sigma_{\pi N \to R}(\sqrt{s}) = \sigma_{\max}(|\mathbf{p}_0/\mathbf{p}|)^2 \frac{0.25\Gamma^2(\mathbf{p})}{0.25\Gamma^2(\mathbf{p}) + (\sqrt{s} - m_0)^2}, \tag{3}$$

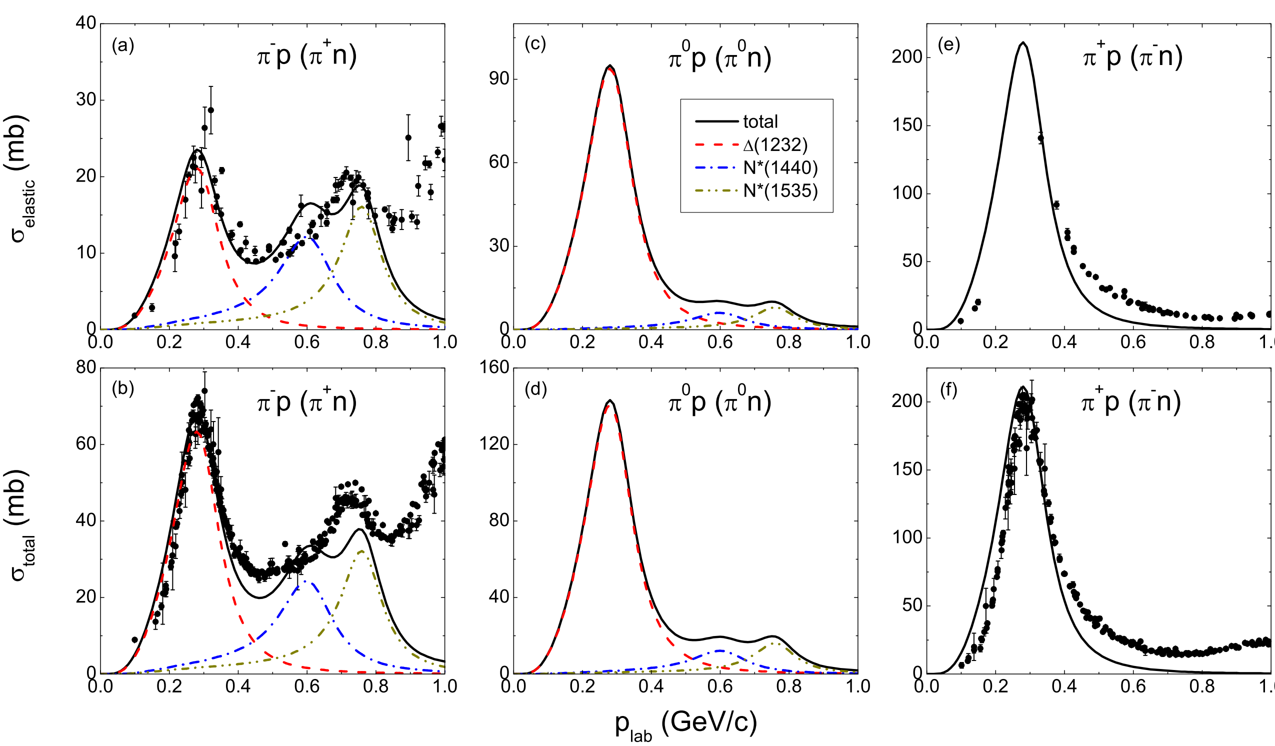

FIG. 2. The elastic (upper panels) and total (lower panels) pion-nucleon scattering cross sections contributed from different resonances. The available data are taken from the PDG Collaboration [28].

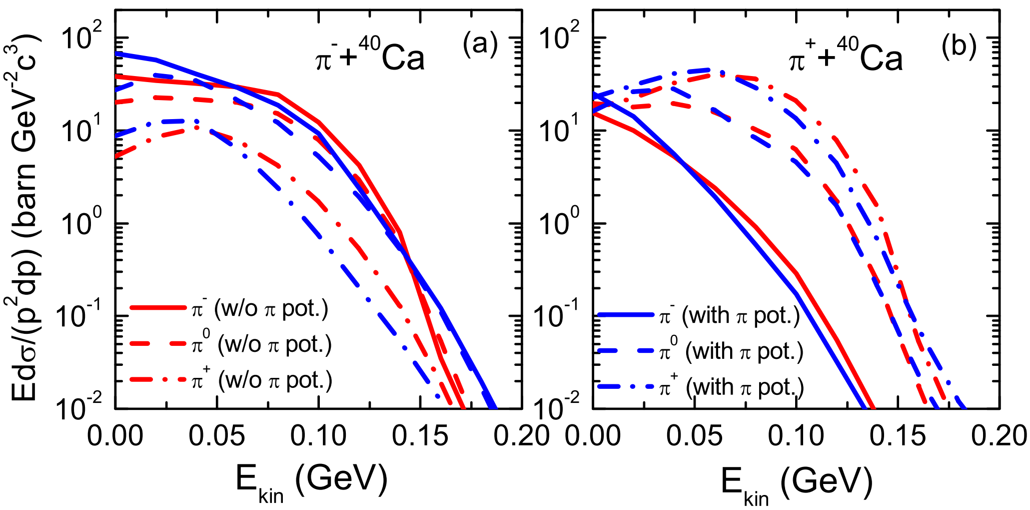

FIG. 3. Kinetic energy spectra of π^-, π^0, and π^+ produced in collisions of π^- and π^+ on ^{40}Ca at an incident momentum of 300 MeV/c without (red lines) and with (blue lines) the pion-nucleon potentials, respectively.

where $\mathbf{p}$ and $\mathbf{p}_0$ are the momenta of pions at the energies of $\sqrt{s}$ and m_0, respectively, and m_0 is the centroid of the resonance mass, e.g., 1.232, 1.44, and 1.535 GeV for $\Delta(1232)$, $N^*(1440)$, and $N^*(1535)$, respectively. The maximum cross section $\sigma_{\max}$ is taken from fitting the total cross sections of the available experimental data in pion-nucleon scattering with the Breit-Wigner form of resonance formation [27]. For example, 200, 133.3, and 66.7 mb for $\pi^+ + p \to \Delta^{++}$ ($\pi^- + n \to \Delta^-$), $\pi^0 + p \to \Delta^+$ ($\pi^0 + n \to \Delta^0$), and $\pi^- + p \to \Delta^0$ ($\pi^+ + n \to \Delta^+$), respectively. And 24, 12, 32, and 16 mb for $\pi^- + p \to N^{*0}(1440)$ [$\pi^+ + n \to N^{*+}(1440)$], $\pi^0 + p \to N^{*+}(1440)$ [$\pi^0 + n \to N^{*0}(1440)$], $\pi^- + p \to N^{*0}(1535)$ [$\pi^+ + n \to N^{*+}(1535)$], and $\pi^0 + p \to N^{*+}(1535)$ [$\pi^0 + n \to N^{*0}(1535)$], respectively. Shown in Fig. 2 is a comparison of the elastic and total cross sections in the pion-nucleon collisions with the available data from the PDG Collaboration [28]. The total cross sections include the sum of three resonances and the contributions of strangeness production. It is obvious that more resonances are needed to be implemented at the pion momentum above 0.5 GeV/c. All possible contributions of nucleonic resonances and strangeness resonances have been included in the Giessen-Boltzmann-Uehling-Uhlenbeck (GiBUU) transport model [29]. The spectra can be reproduced nicely well with the resonance approach, in particular in the domain of Δ-resonance momenta (0.298 GeV/c). The pion-nucleon scattering dominates the energy deposition in the pion-induced reactions, which contributes the fragmentation of target nuclei.

III. RESULTS AND DISCUSSION

Nuclear reactions induced by pions in the Δ-resonance region provide the opportunity to study the pion-nucleon interaction, the charge-exchange reactions, and the in-medium properties of Δ resonance, which are not well understood up to now. Shown in Fig. 3 is the kinetic energy distributions

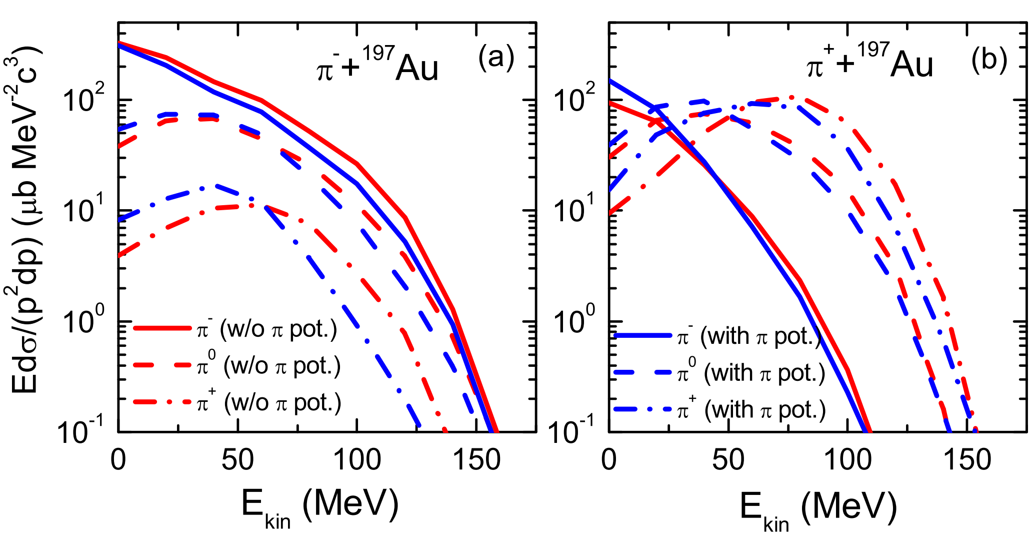

FIG. 4. The same as in Fig. 3, but for the target of ^{197}Au at an incident kinetic energy of 180 MeV.

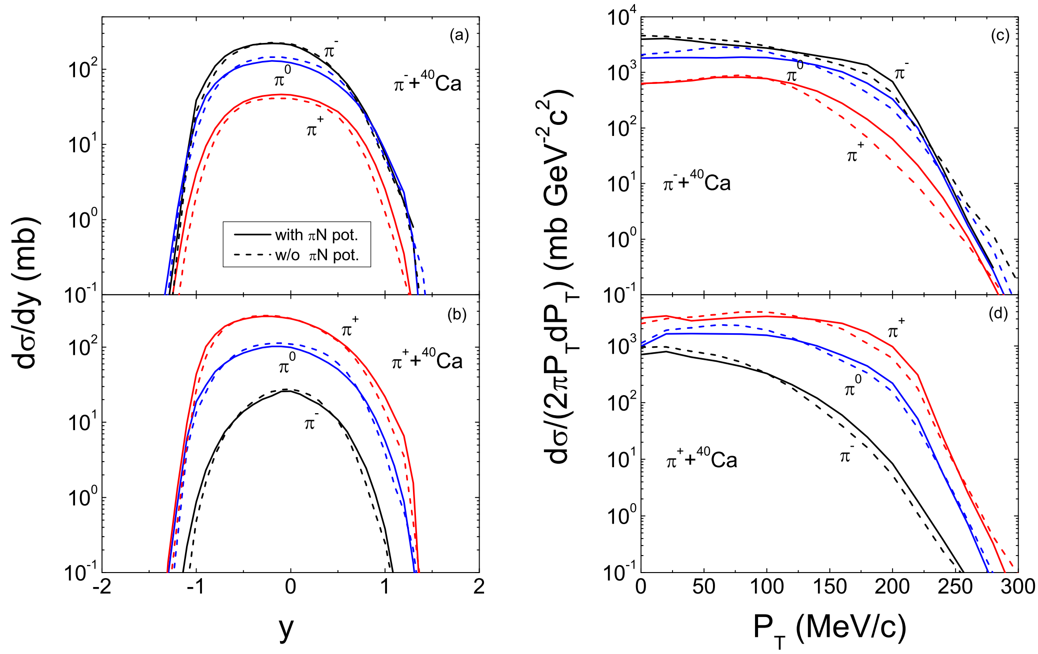

FIG. 5. Rapidity and transverse momentum distributions of π^-, π^0, and π^+ produced in pion-induced reactions at the incident momentum of 300 MeV/c.

of π^-, π^0, and π^+ produced in collisions of π^- and π^+ on ^{40}Ca at the Δ-resonance energy, respectively. The double-charge-exchange reactions $\pi^{\pm}A \to \pi^{\mp}X$ have non-negligible contributions on the pion production. The total multiplicities of π^- and π^+ are 0.55 and 0.12 for the π^--induced reactions and 0.05 and 0.69 for the π^+-induced reactions. The Coulomb interaction between charged pions and protons influences the absorption probability of pions in nuclear medium. The pion-nucleon potential changes the kinetic energy spectra, i.e., reducing the energetic pion production. But the total pion yields weakly depend on the potential. A more pronounced effect from the potential is observed for a heavier target as shown in Fig. 4.

In the past decades, the double-charge exchange (DCX) in pion-induced reactions has attracted much attention, which provided the possibility to explore the multiple-pion interaction in a nucleus, which is involved in two or more nucleons. Shown in Fig. 5 is the rapidity and transverse momentum distributions of pion production on the target of ^{40}Ca at the incident momentum of 300 MeV/c. The structure of pion production from the DCX, single-charge exchange, and elastic scattering is very similar in phase space. The DCX cross sections are lower and depend on isospin ingredients of target nuclei, i.e., $R(\pi^+/\pi^-)$ and $R(\pi^-/\pi^+)$ being 0.22 and 0.07 for the reactions of (π^-,π^+) and (π^+,π^-) on ^{40}Ca, respectively. The ratios are 0.07 and 0.13 for (π^-,π^+) and (π^+,π^-) on ^{197}Au at the same energy. The process (π^-,π^+) can be understood via the reactions associated with at least two protons, e.g., $\pi^- p \to \Delta^0$, $\Delta^0 \to \pi^0 n$, $\pi^0 p \to \Delta^+$, and $\Delta^+ \to \pi^+ n$. In the neutron-rich nuclei, the process is constrained because of the larger collision probabilities between π^- (π^0) and neutrons, which leads to the decrease

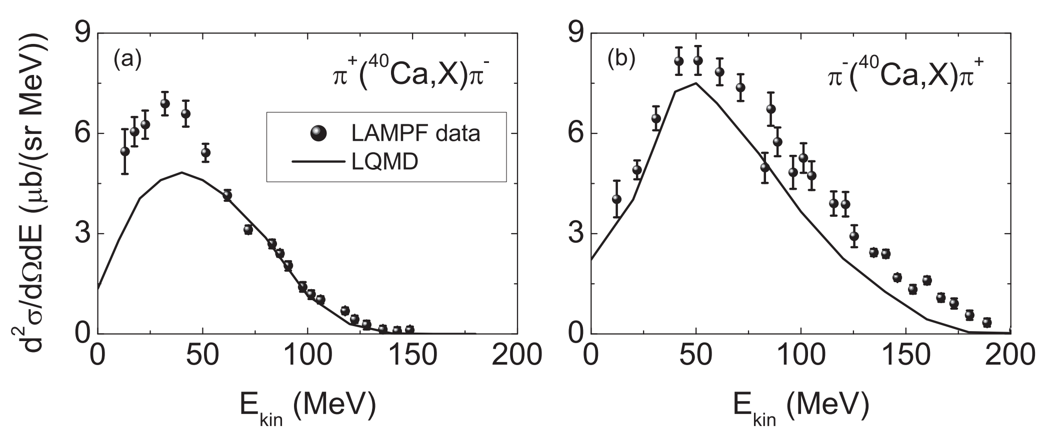

FIG. 6. Kinetic energy spectra of pions at an outgoing angle of 80° in double-charge exchange reactions at an incident energy of 180 MeV. The available data are from the LAMPF measurements [30].

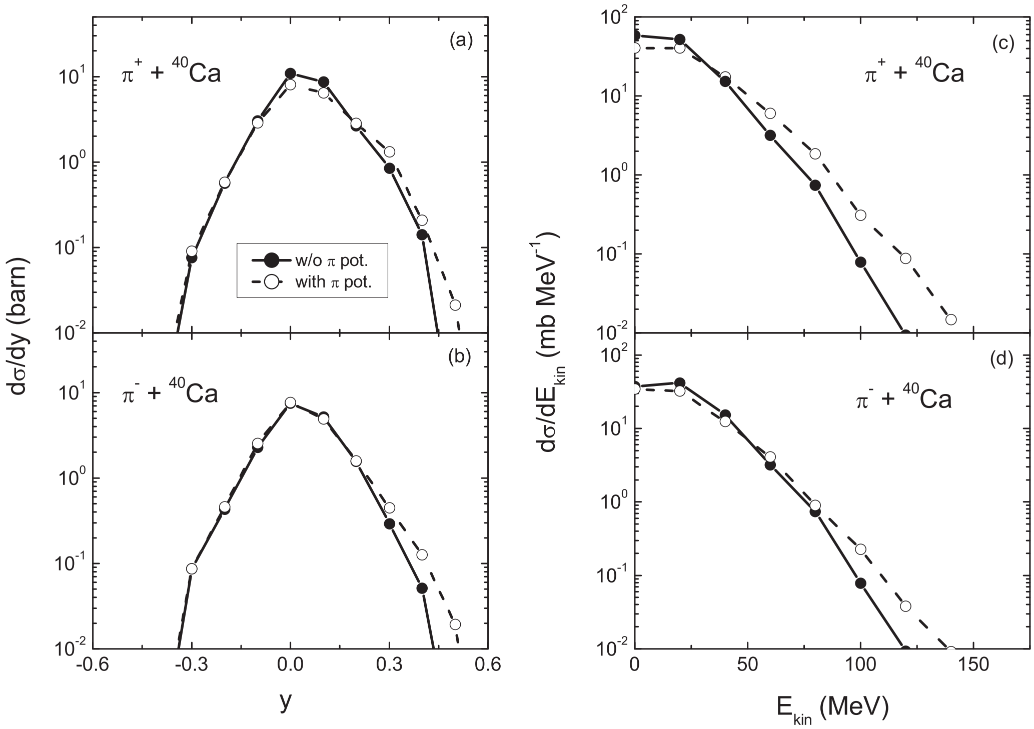

FIG. 7. Rapidity and kinetic energy distributions of fragments with a charge number of $Z \geqslant 2$ in collisions of π^- and π^+ on ^{40}Ca at an incident momentum of 300 MeV/c, respectively.

of the π^+/π^- ratio in the pion DCX reactions. The opposite processes take place for the DCX (π^+,π^-) in the neutron-rich nuclei. The kinetic energy spectra of the pion DCX are calculated as shown in Fig. 6. The consistent trend with the available data at the LAMPF [30] is found. The maximal cross sections move from the kinetic energy of 30 MeV for the DCX (π^+,π^-) to 50 MeV for (π^-,π^+).

The energy deposition in a nucleus by pion-induced reactions is realized via the pion-nucleon collisions associated with the resonance production and reabsorption, which leads

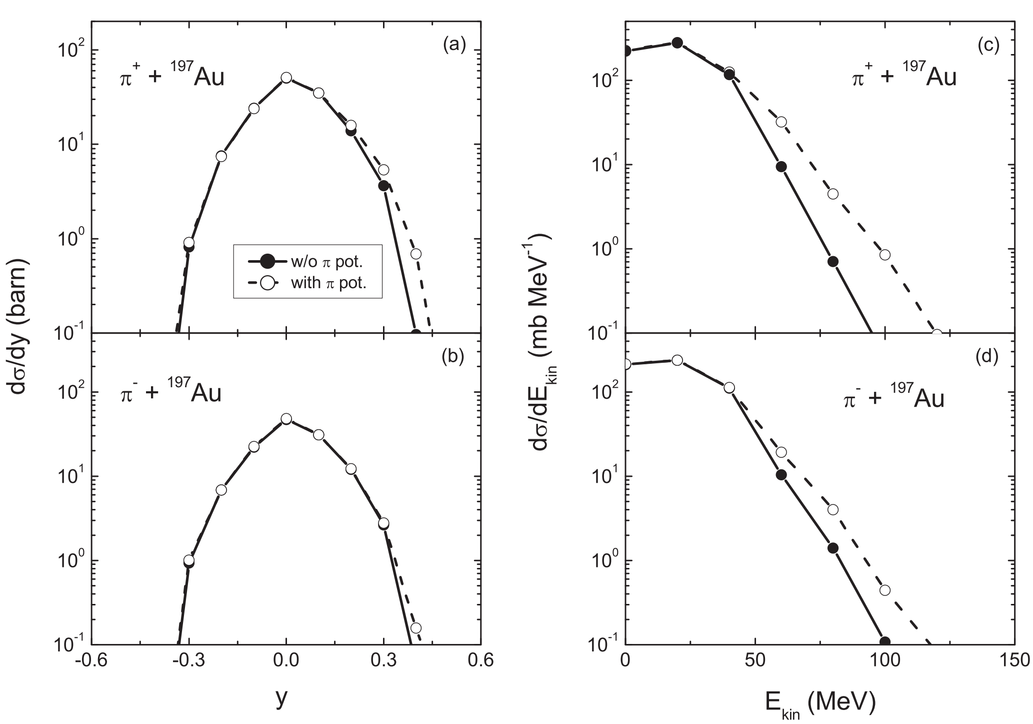

FIG. 8. The same as in Fig. 5, but for the target of ^{197}Au at an incident kinetic energy of 180 MeV.

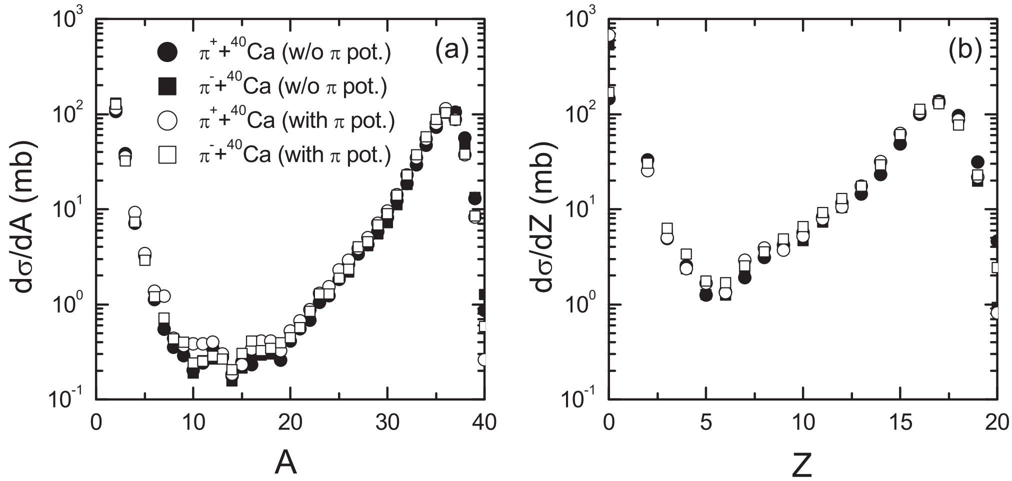

FIG. 9. Mass and charge distributions of fragments produced in collisions of π^- and π^+ on ^{40}Ca at the incident momentum of 300 MeV/c, respectively.

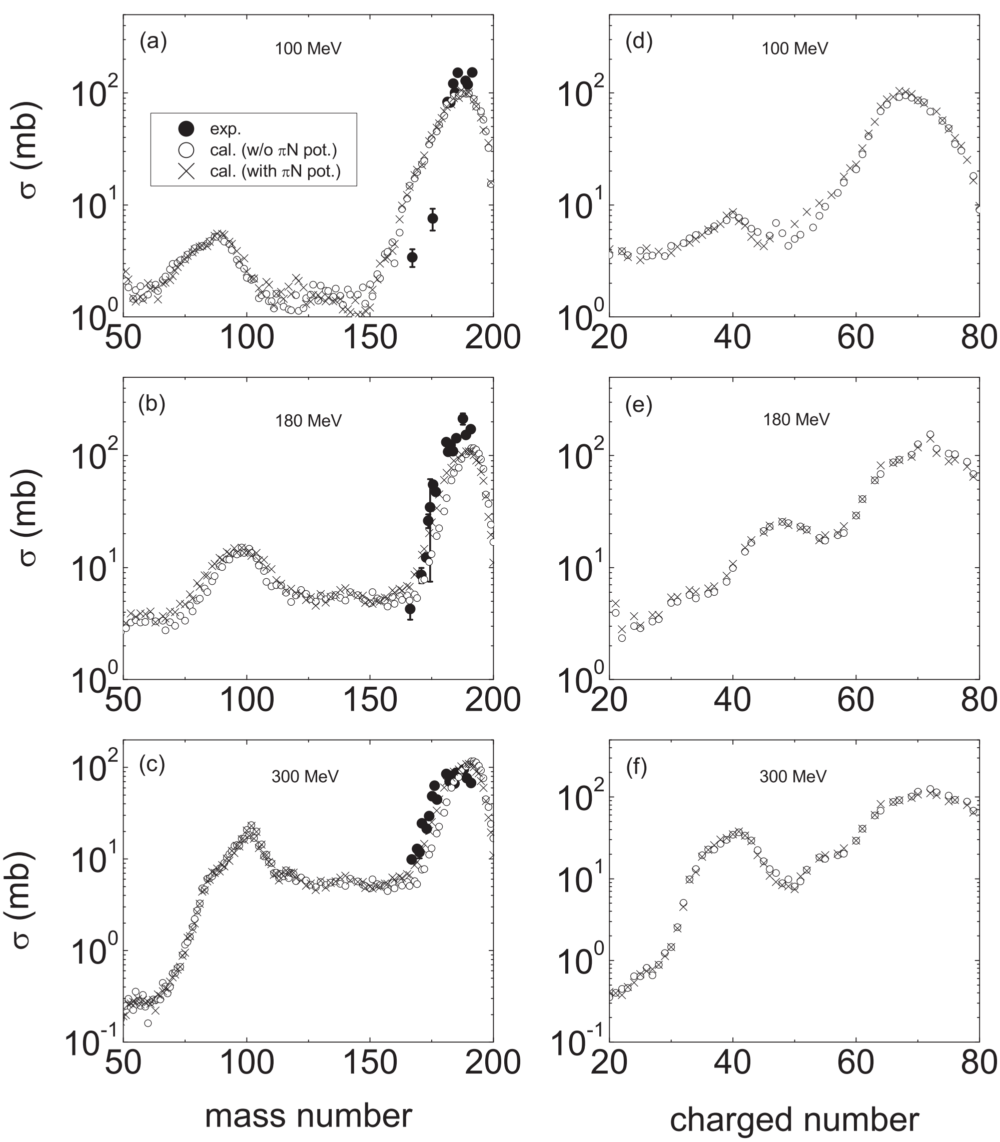

FIG. 10. Fragment distributions with and without the pion-nucleon potential in the $\pi^- + ^{197}$Au reaction at incident energy of 100 MeV, 180 MeV and 300 MeV, respectively. The available data are from the LAMPF measurements [11].

to the formation of a highly excited nucleus. The fragmentation reactions induced by pions are described with the help of the LQMD transport model combined with the GEMINI statistical decay code for excited fragments [31]. The nuclear dynamics is described by the LQMD model. The primary fragments formed at the freeze-out stage are constructed in phase space with a coalescence model, in which nucleons are considered to belong to one cluster with the relative momentum smaller than P_0 and with the relative distance smaller than R_0 (here $P_0 = 200$ MeV/c and $R_0 = 3$ fm). The freeze-out stage is assumed when the energy deposition reaches equilibrium and the pions do not interact with nucleons at the evolution of 300 fm/c taken in this work. The excitation energies of primary fragments are evaluated from the binding energy difference between the fragments and their ground state. The deexcitation of the primary fragments leads to a broad mass distribution, in which the structure effects (shell correction, fission barrier, particle separation energy) contribute to the process. The phase-space distributions of fragments with charge numbers of $Z \geqslant 2$ in collisions of charged pions on ^{40}Ca is calculated as shown Fig. 7. It is interesting that the pion-nucleon potential enhances the fragment production in the domain of high kinetic energy (>60 MeV), which is caused by the fact that the attractive potential increases the energy deposition, in particular, for the π^+-induced reactions. Similar conclusions are found with the heavier target ^{197}Au as shown in Fig. 8.

Fragmentation of target nucleus induced by pions is associated with the pion-nucleon scattering, Δ production and decay process, Δ-nucleon interaction etc. The mechanism is related to the fast nucleon emission, particle evaporation after equilibrium, fission etc. Shown in Fig. 9 is the fragment distributions in π^- and π^+ induced reactions on ^{40}Ca at an incident momentum of 300 MeV/c. It is obvious that the pion-nucleon potential has negligible contribution on

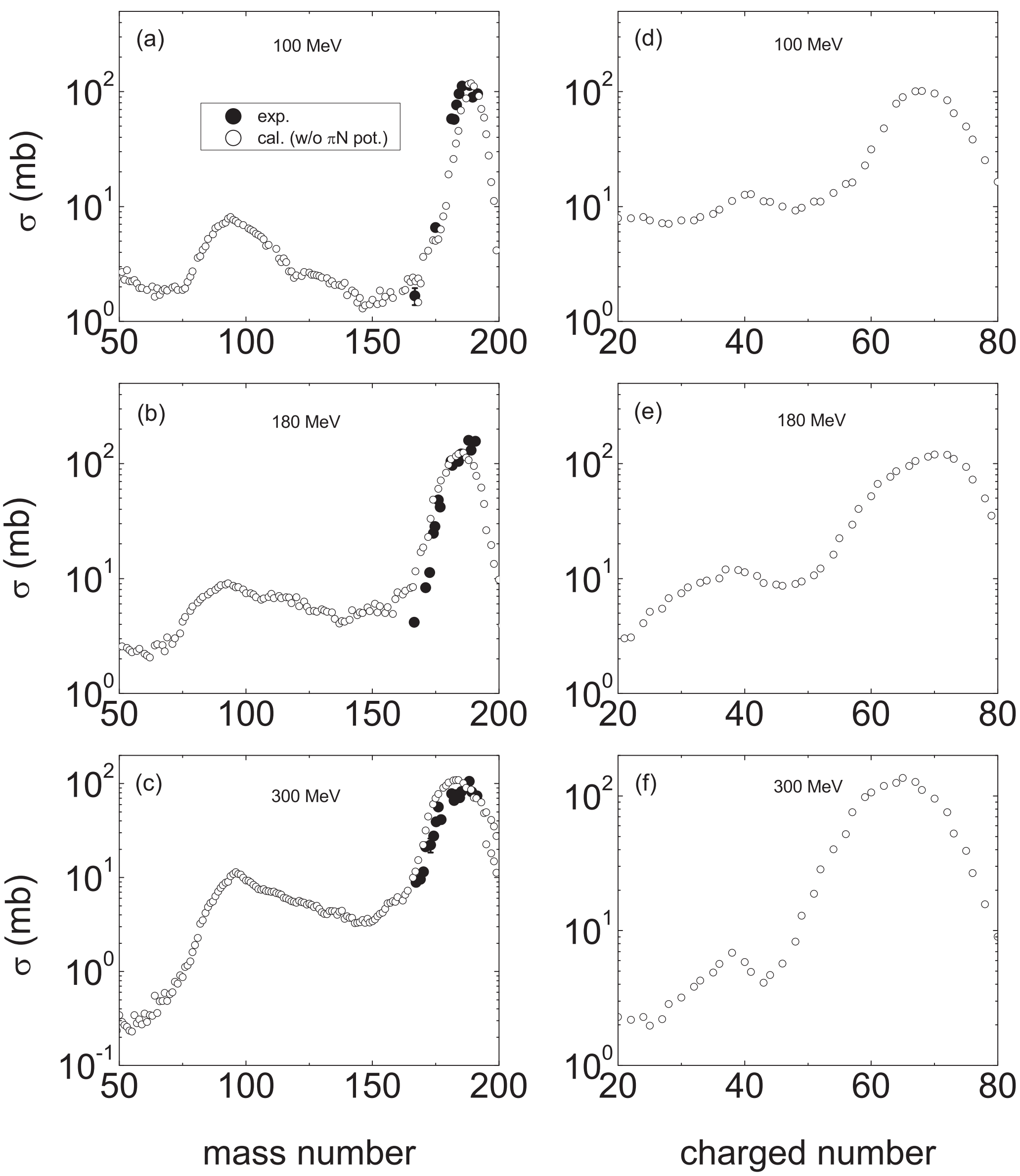

FIG. 11. The same as in Fig. 8, but for the reaction of $\pi^+ + {}^{197}$Au.

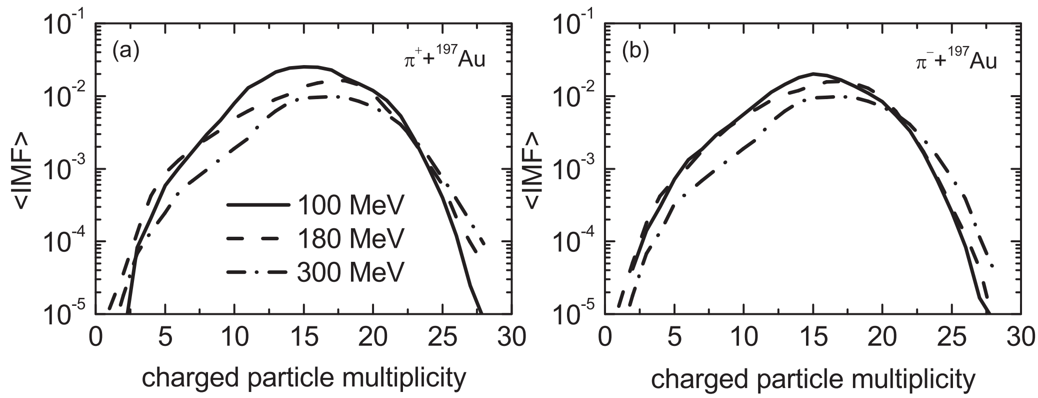

FIG. 12. Correlation of the IMFs and charged-particle multiplicity in collisions of $\pi^{\pm} + ^{197}$Au at incident energies of 100, 180, and 300 MeV, respectively.

the fragment formation. The average mass removals are 4.8 and 4.7 for π^- and π^+, respectively, which are evaluated from $\triangle A = A_T - \int_{A_{\min}}^{A_T} \sigma(A) A dA / \int_{A_{\min}}^{A_T} \sigma(A) dA$. Here, A_T and $A_{\min}$ are the mass numbers of the target nucleus with the integration limit being $A_T/2$. Comparison of calculations with the available experimental data from the LAMPF [11] is shown in Fig. 10 for the π^--induced reactions and in Fig. 11 for bombarding ^{197}Au with π^+ at the incident energies of 100, 180, and 300 MeV. The fragment production in the target-mass region is nicely reproduced. The bump structure of intermediate-mass fragments comes from the fission of heavy fragments. Similar mass and charge distributions are found for both π^-- and π^+-induced reactions.

Emission of the intermediate-mass fragments (IMFs) is caused from the fluctuation of the composite system, which has been investigated by extracting the nuclear equation of state and the density dependence of symmetry energy in heavy-ion collisions [32,33]. I presented a comparison of IMFs correlated to charged-particle multiplicity in pion-induced reactions at different incident energies as shown Fig. 12. Production of the IMFs appears to be maximal near the charged-particle multiplicity of 15. The IMF production is strongly suppressed in the pion-induced reactions in comparison to heavy-ion collisions. It should be noticed that the shadow of fission products dominates the IMF production in the pion reactions. However, the fluctuation of nucleus-nucleus collisions leads to the multifragmentation of colliding partners in heavy-ion collisions, which contributes to the IMF production. The fragmentation reactions induced by pions provide the basis for understanding the pion-nucleon interaction, energy deposition, fragment formation, etc., which are helpful for investigating the hypernucleus production with high-energy pion beams. The hypernucleus formation in pion-nucleus collisions is in progress.

IV. CONCLUSIONS

The fragmentation mechanism and the charge-exchange reactions in pion-induced nuclear reactions have been investigated within an isospin- and momentum-dependent hadron-transport model (LQMD). The pion-nucleon potential is of importance in the pion dynamics in the charge-exchange reactions. The isospin ratio in the pion DCX is influenced by the isospin ingredient of the target nucleus. The attractive pion-nucleon potential near the Δ-resonance energies ($E = 0.19$ GeV, $p = 0.298$ GeV/c) influences the kinetic energy spectra, but has a negligible contribution to the fragmentation process. The relative motion energy is deposited in the nucleus via the pion-nucleon collisions. The transferred energy weakly depends on the incident pion energy. The pion-induced reactions could be performed in the future at facilities such as GSI Facility for Antiproton and Ion Research (Germany), HIAF (IMP, China), etc.

ACKNOWLEDGMENTS

This work was supported by the Major State Basic Research Development Program in China (Grant No. 2015CB856903), the National Natural Science Foundation of China Projects (Grants No. 11675226, No. 11175218, and No. U1332207), and the Youth Innovation Promotion Association of the Chinese Academy of Sciences.

[1] G. Ferini, T. Gaitanos, M. Colonna, M. Di Toro, and H. H. Wolter, Phys. Rev. Lett. **97**, 202301 (2006); M. Di Toro, V. Baran, M. Colonna, and V. Greco, J. Phys. G: Nucl. Part. Phys. **37**, 083101 (2010).
[2] Z. G. Xiao, B. A. Li, L. W. Chen, G. C. Yong, and M. Zhang, Phys. Rev. Lett. **102**, 062502 (2009).
[3] Z. Q. Feng and G. M. Jin, Phys. Lett. B **683**, 140 (2010).
[4] W. J. Xie, J. Su, L. Zhu, and F. S. Zhang, Phys. Lett. B **718**, 1510 (2013).
[5] G. Ferini, M. Colonna, T. Gaitanos, and M. Di Toro, Nucl. Phys. A **762**, 147 (2005).
[6] T. Song and C. M. Ko, Phys. Rev. C **91**, 014901 (2015).
[7] L. Xiong, C. M. Ko, and V. Koch, Phys. Rev. C **47**, 788 (1993).
[8] C. Fuchs, L. Sehn, E. Lehmann, J. Zipprich, and A. Faessler, Phys. Rev. C **55**, 411 (1997).
[9] J. Hong and P. Danielewicz, Phys. Rev. C **90**, 024605 (2014).
[10] Z. Q. Feng and G. M. Jin, Phys. Rev. C **82**, 044615 (2010).

[11] S. B. Kaufman, E. P. Steinberg, and G. W. Butler, Phys. Rev. C **20**, 2293 (1979).
[12] J. Källne, R. C. Minehart, R. R. Whitney, R. L. Boudrie, J. B. McClelland, and A. W. Stetz, Phys. Rev. C **28**, 304 (1983).
[13] K. A. Aniol *et al.*, Phys. Rev. C **33**, 208 (1986).
[14] D. P. Rosenzweig, J. F. Amann, R. L. Boudrie, K. G. R. Doss, D. M. Drake, I. Halpern, M. A. Khandaker, J. Nelson, D. W. Storm, D. R. Tieger, and S. A. Wood, Phys. Rev. C **46**, 1968 (1992).
[15] W. Fong *et al.*, Phys. Rev. C **75**, 064605 (2007).
[16] R. E. Mischke, A. Blomberg, P. A. M. Gram, J. Jansen, J. Zichy, J. Bolger, E. Boschitz, C. H. Q. Ingram, and G. Pröbstle, Phys. Rev. Lett. **44**, 1197 (1980).
[17] K. Ieki *et al.*, Phys. Rev. C **92**, 035205 (2015).
[18] A. P. Krutenkova, T. Watanabe, D. Abe, Y. Fujii, O. Hashimoto, V. V. Kulikov, T. Nagae, M. Nakamura, H. Noumi, H. Outa, P. K. Saha, T. Takahashi, and H. Tamura, Phys. Rev. C **72**, 037602 (2005).
[19] A. Engel, W. Cassing, U. Mosel, M. Schäfer, and Gy. Wolf, Nucl. Phys. A **572**, 657 (1994).
[20] O. Buss, L. Alvarez-Ruso, A. B. Larionov, and U. Mosel, Phys. Rev. C **74**, 044610 (2006).
[21] T.-S. H. Lee and R. P. Redwine, Annu. Rev. Nucl. Part. Sci. **52**, 23 (2002).
[22] Z. Q. Feng, Phys. Rev. C **84**, 024610 (2011).
[23] Z. Q. Feng, Phys. Rev. C **85**, 014604 (2012); Nucl. Phys. A **878**, 3 (2012); Phys. Lett. B **707**, 83 (2012).
[24] Z. Q. Feng and H. Lenske, Phys. Rev. C **89**, 044617 (2014); Z. Q. Feng, *ibid.* **93**, 041601(R) (2016).
[25] Z. Q. Feng, W. J. Xie, P. H. Chen, J. Chen, and G. M. Jin, Phys. Rev. C **92**, 044604 (2015); Z. Q. Feng, arXiv:1606.01083.
[26] S. Huber and J. Aichelin, Nucl. Phys. A **573**, 587 (1994); Z. Q. Feng and G. M. Jin, Chin. Phys. Lett. **26**, 062501 (2009).
[27] B. A. Li, A. T. Sustich, B. Zhang, and C. M. Ko, Int. J. Mod. Phys. E **10**, 267 (2001).
[28] K. A. Olive *et al.* (Particle Data Group Collaboration), Chin. Phys. C **38**, 090001 (2014).
[29] O. Buss *et al.*, Phys. Rep. **512**, 1 (2012).
[30] S. A. Wood, J. L. Matthews, E. R. Kinney, P. A. M. Gram, G. A. Rebka, and D. A. Roberts, Phys. Rev. C **46**, 1903 (1992).
[31] R. J. Charity *et al.*, Nucl. Phys. A **483**, 371 (1988).
[32] T. X. Liu, M. J. van Goethem, X. D. Liu *et al.*, Phys. Rev. C **69**, 014603 (2004); M. A. Famiano, T. Liu, W. G. Lynch, M. Mocko, A. M. Rogers, M. B. Tsang, M. S. Wallace, R. J. Charity, S. Komarov, D. G. Sarantites, L. G. Sobotka, and G. Verde, Phys. Rev. Lett. **97**, 052701 (2006).
[33] Z. Q. Feng, Phys. Rev. C **94**, 014609 (2016).